Nanoparticle Catalysis

DOI: 10.1002/anie.201106515

Thermosensitive Au-PNIPA Yolk–Shell Nanoparticles with Tunable Selectivity for Catalysis**

*Shuang Wu, Joachim Dzubiella, Julian Kaiser, Markus Drechsler, Xuhong Guo, Matthias Ballauff, and Yan Lu**

Metallic nanoparticles have been the subject of intense research recently because of their catalytic properties, which may differ considerably from the bulk metal.[1–3] As the free nanoparticles tend to aggregate and are difficult to handle in catalytic applications, colloidal carrier systems have been developed that encapsulate and stabilize the particles.[4,5] More recently, so-called smart carrier systems, such as thermosensitive microgels,[6–9] have become the focus of research. These hybrids react on external stimuli and allow the catalytic properties to be altered accordingly. Thus, thermosensitive polystyrene (PS)-poly(*N*-isopropylacrylamide) (PNIPA) core–shell microgels were applied as the active nanoreactor for the immobilization of metal nanoparticles.[10] The catalytic activity of immobilized metal nanoparticles can be tuned by the swelling and shrinking of the microgels.[11] Liz-Marzán et al.[12] have developed a Au-PNIPA core–shell colloidal system. They found that the thermoresponsive PNIPA shell with limited cross-linking allows for particularly efficient control of the catalysis of encapsulated Au nanoparticles.[13]

Recently, yolk–shell structures that consist of a single metal nanoparticle within an inorganic[14–17] or polymeric shell[18,19] have become the subject of intense research. These systems can be used to tune the catalytic activity of the enclosed nanoparticle by a suitable architecture of the shell. Yolk–shell structures have the clear advantages in that individual metal nanoparticles are enclosed in a compartment that prevents aggregation with other nanoparticles. Furthermore, the embedded gold nanoparticle has a free surface that is not blocked by any surface group or polymer compared to the Au-PNIPA core–shell system. Moreover, the permeability of the shell may be tuned to a certain extent. Therefore, yolk–shell systems may be regarded as true nanoreactors that allow the catalytic activity of single nanoparticles to be studied in a defined environment.

Herein we present a thermosensitive yolk–shell system that uses temperature as a trigger for reaction. Figure 1a shows the underlying principle of these systems: A single Au nanoparticle is encapsulated in a hollow thermosensitive PNIPA shell. The porosity and the hydrophobicity of this shell can be tuned in a well-defined manner by temperature while the colloidal stability of the entire hybrid is fully maintained. We show this by monitoring the reduction of hydrophilic 4-

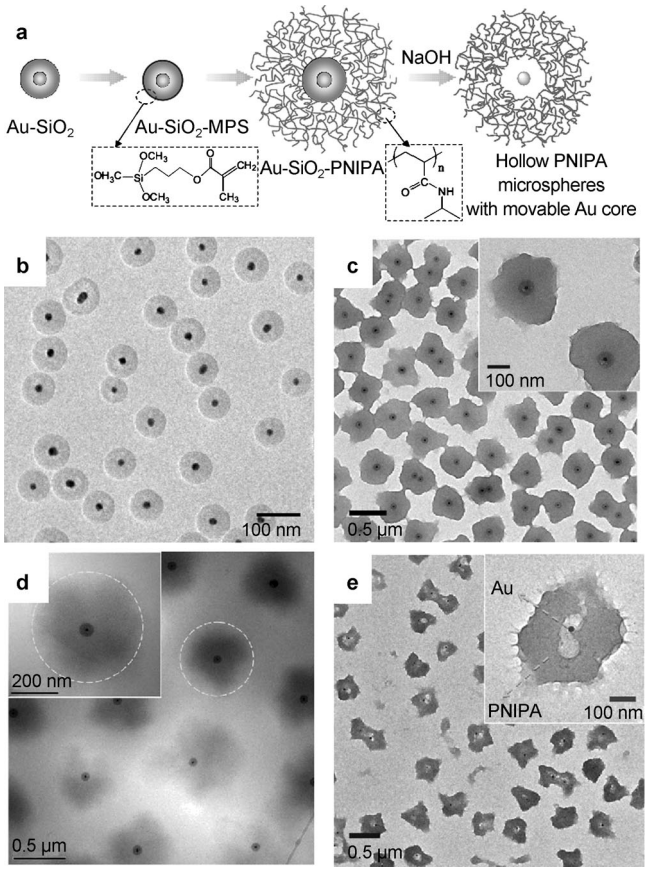

Figure 1. a) Illustration of the generation of Au-PNIPA yolk–shell composite particles (for details, see text). b,c) TEM images of b) Au-SiO_2 core–shell nanoparticles and c) Au-SiO_2-PNIPA trilayer composites. d) Cryo-TEM image of Au-SiO_2-PNIPA composites. e) TEM image of Au-PNIPA yolk–shell particles after the removal of silica.

[*] S. Wu, Prof. X. Guo
State-Key Laboratory of Chemical Engineering
East China University of Science and Technology
200237 Shanghai (China)
S. Wu, Prof. J. Dzubiella, J. Kaiser, Prof. M. Ballauff, Dr. Y. Lu
F-I2 Soft Matter and Functional Materials
Helmholtz-Zentrum Berlin für Materialien und Energie
14109 Berlin (Germany)
and
Institut für Physik, Humboldt-Universität zu Berlin
12489 Berlin (Germany)
E-mail: yan.lu@helmholtz-berlin.de
Dr. M. Drechsler
Makromolekulare Chemie II, University of Bayreuth
95440 Bayreuth (Germany)

[**] The authors thank the Deutsche Forschungsgemeinschaft, Schwerpunktprogramm "Hydrogele" (SPP1259) and the 111 Project Grant B08021 for financial support.

Supporting information for this article is available on the WWW under http://dx.doi.org/10.1002/anie.201106515.

nitrophenol[20] and the more hydrophobic nitrobenzene by sodium borohydride.[21] Moreover, the combination of these reactions can be used to study the selectivity of a catalyst. All data derived herein will demonstrate that the thermosensitive yolk–shell particles provide a novel system in which the selectivity of the enclosed metal nanoparticles can be tuned by temperature.

The Au-PNIPA yolk–shell particles can be synthesized in three steps as shown in Figure 1a. The Au-SiO_2 core–shell particles and the modification with 3-(trimethoxysilyl)propyl methacrytate (MPS) were made according to method reported by Liz-Marzán et al.[22,23] and Hellweg et al.[24] (see the Supporting Information). As shown in Figure 1b, Au particles with diameter of 15 ± 3 nm are homogeneously coated with a silica shell of 26 ± 2 nm thickness. The formation of the PNIPA shell on the Au-SiO_2 particle surface was first confirmed by a TEM image (Figure 1c). Figure 1d shows a cryo-TEM image of the particles. The thickness of the PNIPA shell of about 270 nm agrees well with the thickness of the PNIPA shell determined by DLS at room temperature (marked as a dashed line in Figure 1d). The silica midlayer of the Au-SiO_2-PNIPA composites can be further selectively removed by etching in a highly concentrated NaOH solution.[17] A TEM image (Figure 1e) confirms the yolk–shell structure of the Au-PNIPA particles. DLS measurements of the yolk–shell particles prove the thermoresponsibility of PNIPA shell (Supporting Information, Figure S4).

UV/Vis spectra taken during the catalytic reduction of 4-nitrophenol (4-NP) as well during the reduction of nitrobenzene (NB) are given in the Supporting Information, Figure S5. In the case of 4-NP, the peak at 400 nm, which is due to the 4-nitrophenolate ions, decreases gradually with reaction time, and a new peak appears at 300 nm, which results from product of 4-aminophenol. In the case of reduction of nitrobenzene (NB) by $NaBH_4$,[21] the characteristic absorption peak of NB at 275 nm weakens with reaction time and the absorption peak of aminobenzene (AB) at 232 nm increases gradually, which indicates the reduction of NB to AB. The kinetic analysis of both reactions can be carried out as described in detail recently from the temporal decay of these peaks in terms of a rate constant k_1, which is normalized to the entire surface S present in the system (cf. Ref. [20] and Supporting Information, Figure S5).

The catalytic activity of Au-PNIPA yolk–shell particles has been measured as a function of temperature T for the reductions of 4-NP and NB, respectively. As shown in Figure 2a, the rate constants do not follow a simple Arrhenius law with constant activation energy. This behavior must be assigned to the strong temperature dependence of both the overall size of the network (compare with Figure 2a) and its physicochemical properties. In particular, right at the LCST of the PNIPA shell the rate shows a local minimum, which is similar to the results reported for metal nanoparticles immobilized in PS-PNIPA core–shell particles.[25,26] However, the overall rate of reduction of NB dramatically increases when above the LCST, such that a remarkable inversion takes places from a 4-NP-favored reduction at small $T <$ LCST to a NB-favored reduction at large $T >$ LCST.

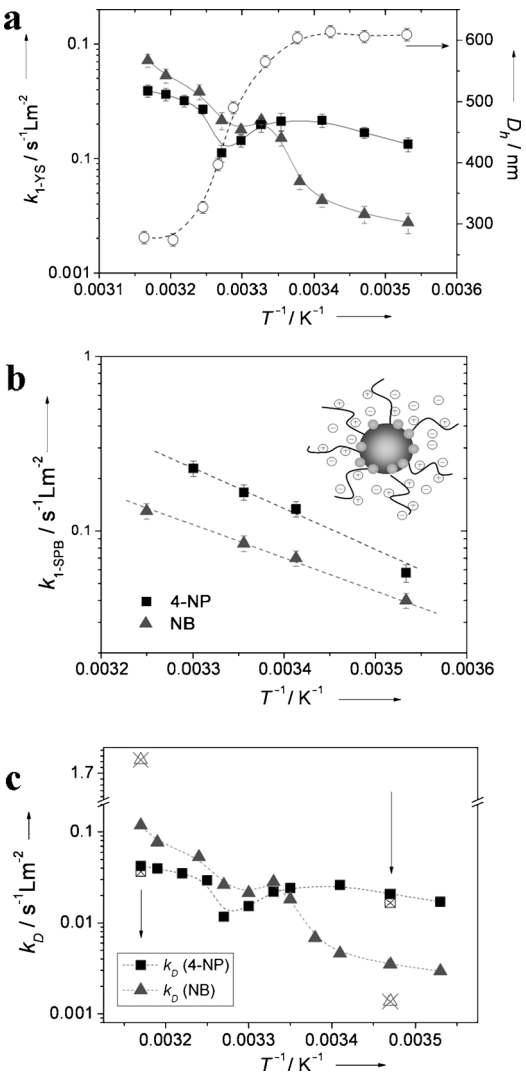

Figure 2. Arrhenius plots of the reaction rate constant k_1 (the apparent rate constant k_{app} normalized to surface area of Au nanocatalyst immobilized a) in the yolk–shell carriers (this work) and b) in non-thermosensitive spherical polyelectrolyte brushes (SPB). Rectangles: reduction of 4-NP; triangles: reduction of NB; open circles: hydrodynamic diameter (D_h) of Au-PNIPA yolk–shell particles. c) The diffusion-controlled reaction rate k_D [Eq. (1)] vs. $1/T$. The crossed rectangles and triangles indicate the diffusion-controlled rate constant of the reactions in the mixtures of 4-NP and NB performed at 15 °C and 42.5 °C, respectively (see discussion of Figure 4). [4-NP] = 0.1 mM, [NB] = 0.1 mM, [$NaBH_4$] = 10 mM.

To analyze the rate behavior in more detail, we compared the reaction rates to those found for Au nanoparticles immobilized in non-thermosensitive spherical polyelectrolyte brush (SPB) carriers. The structure of these hybrids is shown in Figure 2b: The nanoparticles are immobilized on the surface of core particles of the SPBs. Previous work has suggested that there is virtually no limitation of diffusion in these systems,[20] and a simple linear Arrhenius dependence was obtained for the reduction of both 4-NP and NB (Figure 2b). Moreover, the rate constants are considerably higher than found for the yolk–shell system (compare with Figure 2a). This suggests that diffusion is restricted in the latter system.

To discuss the comparison of both systems in further detail, the rate constant k_{1-YS} can be split into a diffusion-controlled reaction rate k_D and the surface-reaction-controlled rate constant of the free particles that can be approximated by the rate constant k_{1-SPB} measured on the SPB:[13]

$$k_{1-YS}^{-1} = k_{1-SPB}^{-1} + k_D^{-1} = k_{1-SPB}^{-1} + S \cdot \tilde{k}_D^{-1} \quad (1)$$

where $\tilde{k}_D$ is the diffusion controlled rate constant normalized to S, the total surface area of Au nanoparticles normalized to the unit volume of the solution. Figure 2c displays k_D thus obtained with Equation (1). With complete generality, $\tilde{k}_D$ is given by the Smoluchowski–Debye expression:[27]

$$\tilde{k}_D^{-1} = \int_{R_0}^{\infty} \frac{\exp[G(r)/k_B T]}{4\pi D(r) r^2} \, dr \quad (2)$$

where $D(r)$ is the distance-dependent diffusion constant for the particles approaching the reactor and $G(r)$ is the solvation free energy (with respect to the bulk) of the reactants along their pathway to the gold particle with radius R_0. We assume in the following that the reactants have a diffusion constant inside the gel D_g that is much smaller than in the bulk, that is $D_g \ll D_0$, and that there is a transfer free energy ΔG_T from bulk solvent into the gel with inner radius R_1 and outer radius R_2 (Figure 3). Based on these assumptions, Equation (1) can then be solved to yield:

$$\tilde{k}_D \simeq 4\pi D_g R_1 \exp(-\Delta G_T / k_B T) \quad (3)$$

where we neglect terms of order $1/R_2$, since R_0 and $R_1 \ll R_2$. Equation (3) demonstrates that changes in rates are partially governed by changes of D_g in the network but exponentially by changes of the transfer free energy ΔG_T.

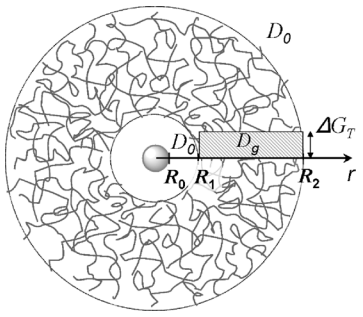

Figure 3. Representation for the model used for the analysis of the kinetic behavior by Equations (2)–(4). See text for details.

As 4-NP and NB are of similar size, their diffusion constant D_g in the gel will be of same magnitude. The major change in the rate for NB when crossing the LCST must then be attributed to significant differences in the affinity of NB to interact with the microgel in its hydrophilic (swollen) state compared to the hydrophobic (collapsed) state. This assumption is consistent with the more hydrophobic nature of molecule NB compared to 4-NP, and a higher number density of NB than 4-NP is expected in the hydrogel (and close to the gold particle) in the collapsed state.

As $\Delta G_T = \Delta H_T - T\Delta S_T$, for $\tilde{k}_D$ it follows that:

$$\ln[\tilde{k}_D] = \ln(4\pi D_g R_1) + \Delta S_T / k_B - \Delta H_T / k_B T \quad (4)$$

which may serve for the analysis of the data in Figure 2c. According to Equation (4), the slopes represent the enthalpic barrier of the reactants imposed by the gel, while the changes in solvation entropy is qualitatively reflected by the intersects of the curves with the k axis.

The slopes in the high- and low-temperature regimes are small and correspond to only 1–2 kJ mol^{-1} transfer (or adsorption) enthalpies ΔH_T. For T slightly below the LCST, the slopes are negative, thus pointing to a quite different adsorption thermodynamics of the gel at the phase transition, where energy fluctuations are maximal. The most significant change, however, is observed for the k axis intercept when NB and 4-NP are compared for high and low temperatures, which must be assigned to changes in the transfer entropy ΔS_T. Indeed it is known that hydrophobic association is entropy-driven; that is, the transfer free energy ΔG is completely dominated by $\Delta S > 0$,[28] which is fully consistent with our picture of hydrophobically promoted rates in the collapsed state for NB. Thus, based on the analysis above, the reaction is diffusion-controlled owing to the slow diffusion of the reactants through the gel network and concomitant solvation barriers, which are very different for the more hydrophobic NB and hydrophilic 4-NP. It is worth noting that above model should be applicable not only to present yolk–shell system but also to the core–shell systems developed by Liz-Marzán.[12,13]

The selectivity of the yolk–shell catalyst can now be tested in an additional experiment in which a mixture of 4-NP and NB is reduced in presence of the catalyst. The kinetics of this reaction can be followed by UV/Vis measurement simultaneously because the characteristic peaks for 4-NP and NB are well separated from each other (Figure 4a). Moreover, the maximum absorbance of NB at 275 nm used for the kinetic analysis is located right above one of the isosbestic points of the reduction of 4-NP. Because of this fortunate fact, the reaction of 4-NP does not disturb the analysis of the 4-NB concentration as the function of time. For a quantitative analysis, we only need to subtract the absorption at the isosbestic point of 4-NP (0.15 at 275 nm) from the NB spectra (see also the Supporting Information, Figure S6).

Kinetic measurements achieved in this way are shown in Figure 4b,c. It is evident that reaction rate for both substrates changes with temperature in the same way as already shown in Figure 2: At low temperatures, 4-NP is reduced much faster, while high temperatures lead to a preferred reduction of NB. However, the rate constant obtained for the reduction of 4-NP ($k_{app} = 7.5 \times 10^{-4}$ s^{-1}) is now one order higher than that of NB ($k_{app} = 7.2 \times 10^{-5}$ s^{-1}) at 15 °C; that is, the selectivity of the reaction is dramatically enhanced in the mixture. A similar enhancement of selectivity is also observed for the reaction at 42.5 °C. The diffusion-controlled reaction rates were calculated from Equation (1) and are marked as crossed rectangles and triangles in Figure 2c. The selectivity of the catalyst toward 4-NP is therefore the same when measured in

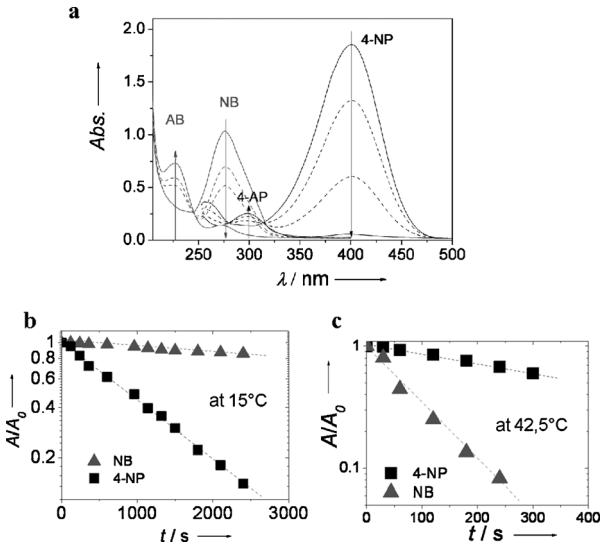

Figure 4. Competitive reduction of 4-nitrophenol (4-NP) and nitrobenzene (NB) by sodium borohydride using Au-PNIPA yolk–shell particles as catalyst. a) UV/Vis absorption spectra as the function of the degree of conversion. Note that the maximum of the NB absorption at 275 nm used for the kinetic analysis is directly above one of the isosbestic points of 4-NP. b,c) Kinetic analysis of the competitive reduction. The reduced absorptions of 4-NP and NB of the mixture is plotted against time t at b) 15 °C and c) 42.5 °C. [4-NP] = 0.1 mM, [NB] = 0.1 mM, [$NaBH_4$] = 10 mM.

this competitive experiment, while the selectivity of the reaction for NB is dramatically enhanced in the mixture, as seen in Figure 2c. Interestingly, at 42.5 °C, the calculated k_D for more hydrophobic molecules NB is even higher than that of k_{1-YS}, indicating that the reaction is no longer diffusion-controlled. Co-solvation effects may be responsible if both substrates are present in the PNIPA network. The present data demonstrate that the reactivity of competitive reactions may be dramatically changed by this yolk–shell catalyst, which opens the way for interesting applications.

In conclusion, we introduce an inorganic–organic hybrid yolk–shell nanostructure that contains a metallic Au nanoparticle as the core and thermosensitive microgel PNIPA as the shell. This hybrid is an effective catalyst for the reduction of 4-nitrophenol and nitrobenzene in aqueous solution. Temperature can be used as a trigger to enhance the selectivity of the catalysis for a given substrate: 4-NP reacts much faster at low temperature, while the reduction of NB is preferred at higher temperature. This selectivity is even enhanced in mixtures of 4-NP and NB. Therfore, yolk–shell systems have a great potential to tailor the catalytic activity and selectivity of metal nanoparticles toward a given reaction.

Experimental Section

Synthesis of Au-SiO_2-MPS nanoparticles: Au-SiO_2 core–shell particles were prepared according to the techniques described by Liz-Marzán.[22,23] In a typical run, an aqueous solution of (3-aminopropyl)trimethosysilane (APS) (0.5 mL, 1 mM) was added to the gold sol (50 mL, 0.5 mM $HAuCl_4$) prepared by the citrate reduction method. Freshly treated active silica (2 mL, 1.08 wt %) was then added to the surface-modified gold sol under vigorous stirring. After 24 h, ethanol (200 mL) was added to above gold solution to make a 1:4 water/ethanol mixture, and then tetraethyl orthosilicate (TEOS; 0.15 mL) and ammonia (1 mL) was introduced into reaction. The reaction solution was allowed to stand for 48 h under stirring. The silica surface was functionalized by of 3-(trimethoxysilyl)propyl methacrylate (MPS; 1.6 mL). As-prepared surface-functionalized Au-SiO_2 nanoparticles were cleaned by centrifugation several times and redispersed in ethanol (2.5 mL). The amount of MPS was calculated and adjusted to obtain a surface density of one molecule per 0.4 nm^{-2}.[24]

Synthesis of Au-SiO_2-PNIPA trilayer composites: In a typical run, Au-SiO_2-MPS core–shell particles in ethanol solution (0.6 mL, 0.085 wt %) was dispersed in poly(vinylpyrrolidone) (M_w = 10000, PVP) (12 mL, 2 wt %) aqueous solution under stirring. After 15 min, NIPA (1.36 wt % of the system) and *N,N′*-methylene-bisacrylamide (BIS) (5 mol % of NIPA) mixture dissolved in water (4 mL) was added inside. The solution was pre-heated to 35 °C under a nitrogen atmosphere and kept stirring for 15 min. Thereafter, the temperature was raised to 70 °C and the polymerization started by the addition of initiator (4.8 mg $K_2S_2O_8$ (KPS) dissolved in 1 mL water). The red emulsion became turbid purple after 10 min and the polymerization lasted for 4 h at 70 °C. The composite particles were then cleaned by centrifugation and redispersion in water several times.

Etching of the silica layer of the Au-SiO_2-PNIPA composite: Au-PNIPA yolk–shell particles were prepared by a silica-etching procedure: NaOH (1 mL, 2 M) solution was added into a Au-SiO_2-PNIPA suspension (4 mL, [Au] = 0.625 mM). The mixture was gently stirred at room temperature overnight and was cleaned by centrifugation (8000 rpm, 15 min).

Catalytic reduction of 4-nitrophenol (4-NP) and nitrobenzene (NB): Sodium borohydride solution (0.5 mL, 0.1 M) was added to a 4-NP or NB solution (4.5 mL, 0.11 mM) contained in a glass vessel. The solution was purged with N_2 to remove oxygen from the system. Thereafter, a given amount of Au-PNIPA particles was added. Immediately after addition of composite particles, UV/Vis spectra of the sample were taken every minute in the range of 250–550 nm for 4-NP and 200–400 nm for NB.

Characterization: UV/Vis spectra were measured with Lambda 650 spectrometer supplied by Perkin-Elmer with a temperature-controlled sample holder with an accuracy of ± 0.1 °C. Transmission electron microscopy (TEM) images were obtained with CM30 Philips microscope operating at an acceleration voltage of 300 kV. Cryogenic transmission electron microscopy was carried out as outlined in Ref. [10]. The swelling behavior of the thermosensitive microgel was determined by Malvern Zetasizer Nano ZS ZEN 3500 at the angle of 173° and was run in the temperature range of 285 K to 340 K.

Received: September 14, 2011
Revised: November 10, 2011
Published online: January 23, 2012

Keywords: metal nanoparticles · nanoparticle catalysis · selectivity · thermosensitive microgels · yolk–shell structures

[1] C. Burda, X. Chen, R. Narayanan, M. A. El-Sayed, *Chem. Rev.* **2005**, *105*, 1025 – 1102.
[2] R. Sardar, M. A. Funston, P. Mulvaney, R. W. Murray, *Langmuir* **2009**, *25*, 13840 – 13851.
[3] D. Astruc, *Nanoparticles and Catalysis*, Wiley-VCH, Weinheim, **2008**.
[4] M. Karg, T. Hellweg, *J. Mater. Chem.* **2009**, *19*, 8714 – 8727.
[5] J. E. Wong, A. K. Gaharwar, D. Müller-Schulte, D. Bahadur, W. Richtering, *J. Colloid Interface Sci.* **2008**, *324*, 47 – 54.
[6] M. A. C. Stuart, W. T. S. Huck, J. Genzer, M. Müller, C. Ocer, M. Stamm, G. B. Sukhorukov, I. Szleifer, V. V. Tsukruk, M. Urban,

F. Winnik, S. Zauscher, I. Luzinov, S. Minko, *Nat. Mater.* **2010**, *9*, 101 – 113.
[7] L. A. Lyon, Z. Meng, N. Singh, C. D. Sorrell, A. St. John, *Chem. Soc. Rev.* **2009**, *38*, 865 – 874.
[8] a) M. Das, L. Mordoukhovski, E. Kumacheva, *Adv. Mater.* **2008**, *20*, 2371 – 2375; b) M. Das, H. Zhang, E. Kumacheva, *Annu. Rev. Mater. Res.* **2006**, *36*, 117 – 142.
[9] R. Pelton, *J. Colloid Interface Sci.* **2010**, *348*, 673 – 674.
[10] a) Y. Lu, M. Ballauff, *Prog. Polym. Sci.* **2011**, *36*, 767 – 792; b) N. Welsch, M. Ballauff, Y. Lu, *Adv. Polym. Sci.* **2010**, *234*, 129 – 163.
[11] a) Y. Lu, Y. Mei, M. Drechsler, M. Ballauff, *Angew. Chem.* **2006**, *118*, 827 – 830; *Angew. Chem. Int. Ed.* **2006**, *45*, 813 – 816; b) Y. Lu, S. Proch, M. Schrinner, M. Drechsler, R. Kempe, M. Ballauff, *J. Mater. Chem.* **2009**, *19*, 3955 – 3961; c) Y. Lu, J. Yuan, F. Polzer, M. Drechsler, J. Preussner, *ACS Nano* **2010**, *4*, 7078 – 7086.
[12] R. Contreras-Cácares, A. Sánchez-Iglesias, M. Karg, I. Pastoriza-Santos, J. Pérez-Juste, J. Pacifico, T. Hellweg, A. Fernández-Barbero, L. M. Liz-Marzán, *Adv. Mater.* **2008**, *20*, 1666 – 1670.
[13] S. Carregal-Romero, N. J. Buurma, J. Pérez-Juste, L. M. Liz-Marzán, P. Hervés, *Chem. Mater.* **2010**, *22*, 3051 – 3059.
[14] K. Kamata, Y. Lu, Y. Xia, *J. Am. Chem. Soc.* **2003**, *125*, 2384 – 2385.
[15] a) P. Arnal, M. Comotti, F. Schüth, *Angew. Chem.* **2006**, *118*, 8404 – 8407; *Angew. Chem. Int. Ed.* **2006**, *45*, 8224 – 8227; b) R. Güttel, M. Paul, F. Schüth, *Catal. Sci. Technol.* **2011**, *1*, 65 – 68.
[16] J. Lee, J. C. Park, H. Song, *Adv. Mater.* **2008**, *20*, 1523 – 1528.
[17] I. Lee, M. A. Albiter, Q. Zhang, J. Ge, Y. Yin, F. Zaera, *Phys. Chem. Chem. Phys.* **2011**, *13*, 2449 – 2456.
[18] G. Liu, H. Ji, X. Yang, Y. Wang, *Langmuir* **2008**, *24*, 1019 – 1025.
[19] G. L. Li, C. A. Tai, K. G. Neoh, E. T. Kang, X. L. Yang, *Polym. Chem.* **2011**, *2*, 1368 – 1374.
[20] a) S. Wunder, F. Polzer, Y. Lu, Y. Mei, M. Ballauff, *J. Phys. Chem. C* **2010**, *114*, 8814 – 8820; b) S. Wunder, Y. Lu, M. Albrecht, M. Ballauff, *ACS Catal.* **2011**, *1*, 908 – 916.
[21] C. Yuan, W. Luo, L. Zhong, H. Deng, J. Liu, Y. Xu, L. Dai, *Angew. Chem.* **2011**, *123*, 3577 – 3581; *Angew. Chem. Int. Ed.* **2011**, *50*, 3515 – 3520.
[22] J. Rodríguez-Fernández, J. Pérez-Juste, F. J. García de Abajo, L. M. Liz-Marzán, *Langmuir* **2006**, *22*, 7007 – 7010.
[23] L. M. Liz-Marzán, M. Giersig, P. Mulvaney, *Langmuir* **1996**, *12*, 4329 – 4335.
[24] M. Karg, I. Pastoriza-Santos, L. M. Liz-Marzán, T. Hellweg, *ChemPhysChem* **2006**, *7*, 2298 – 2301.
[25] Y. Lu, Y. Mei, M. Drechsler, M. Ballauff, *J. Phys. Chem. B* **2006**, *110*, 3930 – 3937.
[26] Y. Mei, Y. Lu, F. Polzer, M. Ballauff, M. Drechsler, *Chem. Mater.* **2007**, *19*, 1062 – 1069.
[27] P. Debye, *Trans. Electrochem. Soc.* **1942**, *82*, 265 – 272.
[28] *Molecular Driving Forces: Statistical Thermodynamics in Chemistry and Biology* (Eds.: K. A. Dill, S. Bromberg, D. Stigter), Taylor Francis, New York, **2003**.

